Featured in Physics

# Scaling Law for Intrinsic Fracture Energy of Diverse Stretchable Networks

Chase Hartquist,[1,*] Shu Wang,[1,*] Qiaodong Cui,[2] Wojciech Matusik,[2,3] Bolei Deng,[4,†] and Xuanhe Zhao[1,‡]

[1]Department of Mechanical Engineering, Massachusetts Institute of Technology, Cambridge, Massachusetts 02139, USA
[2]Inkbit, Medford, Massachusetts 02155, USA
[3]Computer Science and Artificial Intelligence Laboratory, Massachusetts Institute of Technology, Cambridge, Massachusetts 02139, USA
[4]Daniel Guggenheim School of Aerospace Engineering, Georgia Institute of Technology, Atlanta, Georgia 30332, USA

(Received 27 February 2024; revised 28 October 2024; accepted 5 November 2024; published 8 January 2025)

Networks of interconnected materials permeate throughout nature, biology, and technology due to exceptional mechanical performance. Despite the importance of failure resistance in network design and utility, no existing physical model effectively links strand mechanics and connectivity to predict bulk fracture. Here, we reveal a scaling law that bridges these levels to predict the intrinsic fracture energy of diverse stretchable networks. Simulations and experiments demonstrate its remarkable applicability to a breadth of strand constitutive behaviors, topologies, dimensionalities, and length scales. We show that local strand rupture and nonlocal energy release contribute synergistically to the measured intrinsic fracture energy in networks. These effects coordinate such that the intrinsic fracture energy scales independent of the energy to rupture a strand; it instead depends on the strand rupture force, breaking length, and connectivity. Our scaling law establishes a physical basis for fracture of homogeneous networks with uniform strand mechanics and lattice connectivity throughout. The scaling also extends generally for fabricating tough materials from homogeneous networks across multiple length scales.

DOI: 10.1103/PhysRevX.15.011002 Subject Areas: Mechanics, Metamaterials, Soft Matter

## I. INTRODUCTION

Networks ubiquitously underpin the composition of materials throughout nature and daily life, spanning from nanoscale polymers and biological materials [1–7] through microscale architected materials [8–12], synthetic tissues [13,14], and structural networks [15–17] to macroscale fabrics and meshes [18]. The core of designing and selecting network materials that endure routine stresses in nature, technology, and daily life lies in circumventing mechanical fracture [19–22]. Intrinsic fracture energy ($\Gamma_0$)—the lowest energy required to propagate a crack per unit of created surface area—is the key property that characterizes a material's fatigue resistance [23,24]. Despite its importance, no quantitative model accurately predicts the intrinsic fracture energy of networks across multiple length scales from the mechanical behavior and connectivity of their constituents.

A recent study discovered that nonlocal phenomena contribute to intrinsic fracture energy in polymerlike networks with strands exhibiting pronounced strain-stiffening profiles [25]. However, many common or architected network materials contain stretchable strands with different constitutive laws, including linear, bilinear, neo-Hookean, etc. Here, we report a new scaling law for the intrinsic fracture energy of diverse stretchable networks including but not limited to polymerlike networks through combined simulation and experiments:

$$\Gamma_0/M \propto f_f L_f, \tag{1}$$

where $\Gamma_0$ is the intrinsic fracture energy, $M$ is the areal density of strands, $f_f$ is the strand breaking force, and $L_f$ is the stretched strand length at the breaking point. We show that this result applies across multiple length scales ranging from 1 nm to 1 m for networks comprised of stretchable elastic strands with varying single-strand force-length constitutive behaviors ranging from linear to highly nonlinear relations. We similarly demonstrate the scaling law

*These authors contributed equally to this work.
†Contact author: bolei.deng@gatech.edu
‡Contact author: zhaox@mit.edu

is applicable to a breadth of two- and three-dimensional network architectures, including triangular, square, hexagonal, diamond cubic, body-centered cubic, and cubic lattices. Experiments ranging from nanoscale polymer networks to macroscopic architected materials paired with simulations of networks across length scales collectively validate this scaling law.

## II. ASSEMBLING DIVERSE NETWORKS

We connect the intrinsic fracture energy of networks to the constitutive behavior of individual strands by directly assembling and testing diverse networks. Mechanically identical strands with the same initial length $L_0$, terminal length $L_f$, and rupture force $f_f$ comprise each network [see Fig. 1(a)]. To describe strands with force-length behaviors varying from linear to nonlinear, we adopt the modified freely jointed chain (m-FJC) model, which relates the force $f$ and length $L$ as

$$\frac{L}{L_x} = \left[\coth\left(\frac{f}{K_1}\right) - \frac{K_1}{f}\right]\left(1 + \frac{f}{K_2}\right), \tag{2}$$

where the two moduli $K_1$ and $K_2$ describe the stiffnesses of the force-length curve before and after a crossover length $L_x$ [26–28]. We then iteratively assemble strands—each with identical elastic constitutive behavior governed by the m-FJC model—into homogeneous networks for bulk mechanical testing. Homogeneous cases refer to networks with uniform strand mechanics and lattice connectivity throughout. Inhomogeneous networks contain irregularities such as dispersity of strand lengths, mechanical variability between strands, or topological inconsistency through defects like dangling ends. Prior works introduce lattice models [29] to simulate details of brittle fracture [15,30] and mesoscale or quasicontinuum network models to probe aspects of elastomeric fracture [31–35]. The numerical framework simulates a pure shear fracture test to evaluate the critical energy release rate $G_c$ necessary to propagate an edge crack in a notched sample. For networks with elastic strands, the intrinsic fracture energy $\Gamma_0$ matches $G_c$. The simulation first uniaxially loads a notched sample in pure shear from its undeformed height $h_0$ to the critical height $h_c$ that initiates crack growth. The condition for crack initiation matches that of crack propagation in these simulations, since all strands are elastic. The simulation subsequently loads a pristine sample from $h_0$ past $h_c$, recording the nominal stress $s$ as a function of stretched height $h$. It finally computes $\Gamma_0 = \int_{h_0}^{h_c} s dh$, an inherent property of elastic networks with a sufficient number of repeating layers (see details in the Supplemental Material [36]). To ensure the convergence of $\Gamma_0$, we simulate amply large networks with more than 1000 vertical layers of strands. The goal of numerical simulations is to connect the measured network-level intrinsic fracture energy to the preset strand-level force-length constitutive behavior. To achieve that, we systematically tune the strand failure lengths $L_f$ from 1 nm to 1 m and rupture forces $f_f$ from 1 nN to 1 N. While we acknowledge some models for polymers postulate strand softening effects before a strand breaks [27,37], we consider abrupt strand scission [38], as this is supported by the single-molecule force spectroscopy of synthetic polymers [39] and proteins [40]. Similarly, we vary the ratio of $K_2/K_1$ as a nonlinearity parameter to match a breadth of natural and synthetic networks with behavior ranging from linear ($K_2/K_1 \approx 1$) to highly nonlinear ($K_2/K_1 \approx 10^4$) [see Fig. 1(c)]. We intentionally limit our focus to stretchable networks where the breaking stretch of each strand is greater than five (i.e., $L_f > 5L_0$) to minimize geometric artifacts (see Supplemental Material [36] for a detailed explanation).

## III. SCALING FOR NETWORK INTRINSIC FRACTURE ENERGY

We find that all simulation results—across strand lengths, failure forces, and nonlinearities—follow a scaling law: $\Gamma_0/M \propto f_f L_f$. In Fig. 1(d), we plot simulated intrinsic fracture energy per strand $\Gamma_0/M$ against the product of failure force and length of the composite strands $f_f L_f$ and find that all data points collapse along a single straight line: $\Gamma_0/M = \alpha f_f L_f$, where $\alpha$ is a fitting parameter depending on the specific lattice type. While the scaling law holds for arbitrary strand lengths, strand breaking forces, nonlinearity parameters, and network orientations (see Supplemental Material [36] for details), the lattice topology governs the prefactor $\alpha$. The simulation yields $\alpha = 0.73$ for triangular lattices [Fig. 1(d)], $\alpha = 1.46$ for square lattices [top in Fig. 1(e)], and $\alpha = 2.54$ for hexagonal lattices [bottom in Fig. 1(e)].

Additional simulations reveal the generality of this scaling law to three-dimensional networks. We assemble diamond, body-centered cubic (bcc), and cubic lattices [see Figs. 1(f)–1(h)] from strands with the same breadth of behaviors. The scaling law accurately predicts intrinsic fracture energy for each three-dimensional topology. The diamond, bcc, and cubic lattices give $\alpha = 1.07$, $\alpha = 1.74$, and $\alpha = 1.50$, respectively [see Figs. 1(f)–1(h)].

## IV. PHYSICAL EXPLANATION

We next seek to understand the origins of the scaling law $\Gamma_0/M \propto f_f L_f$ by analyzing the fracture process of the bridging strand (i.e., the first breaking strand along the crack plane) and examining its energetic contributions. While loading a notched network to fracture [Figs. 2(a) and 2(c)], the bridging strand at the crack tip stretches from $L_0$ to $L_f$ and stores elastic energy [$U_{\text{strand}}$, Figs. 2(b) and 2(d)]. However, instantaneously following bridging strand rupture, the network remains unbalanced and must release additional energy to reach a new equilibrium. In real

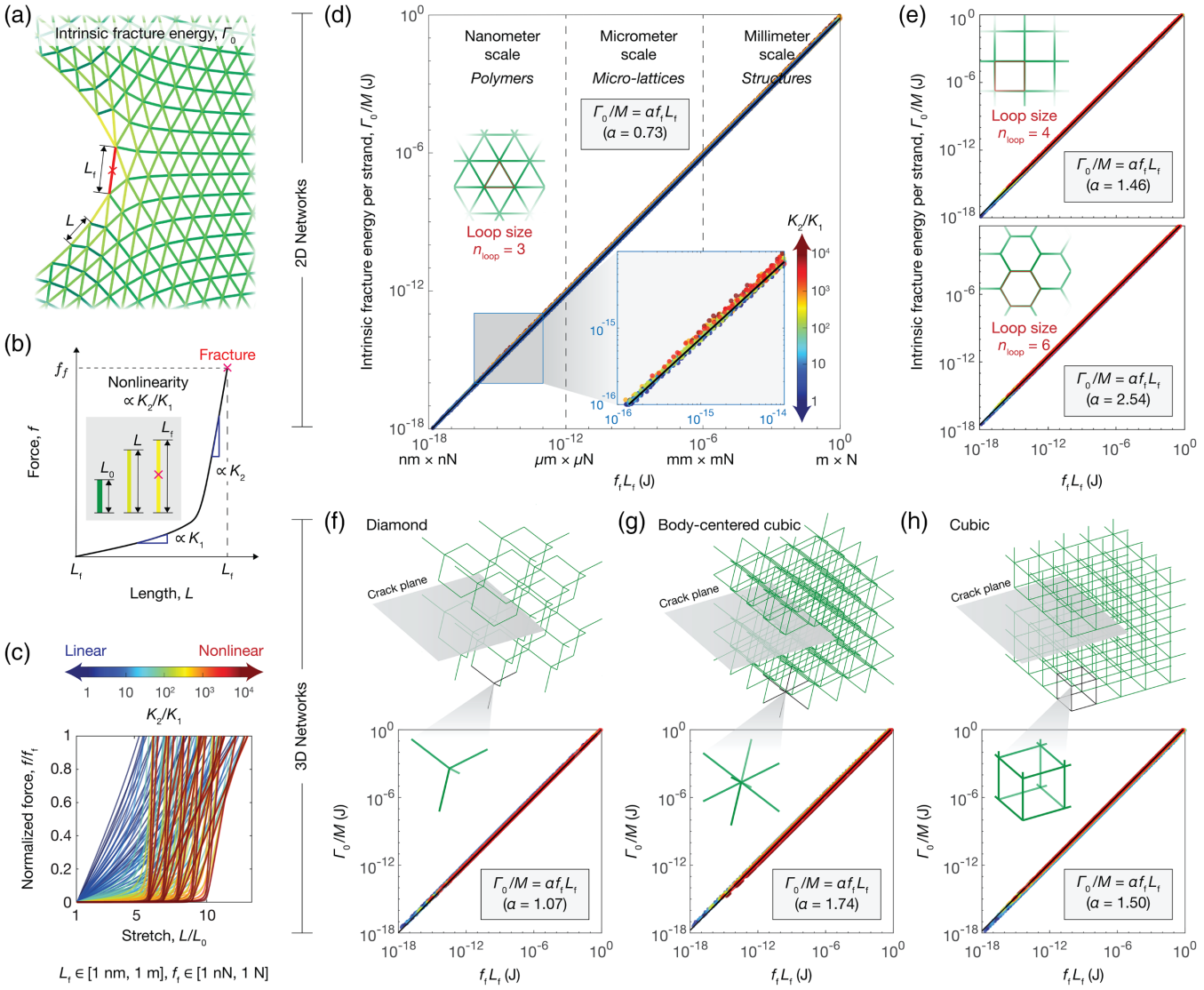


FIG. 1. Scaling law for intrinsic fracture energy of diverse stretchable networks. (a) Collections of identical strands are assembled into networks to measure the intrinsic fracture energy $\Gamma_0$. The crack tip of a loaded, notched specimen depicts how strand lengths ($L$, colored by stored energy) increase during loading as the bridging strand approaches its failure length ($L_f$). (b) The nonlinearity parameter ($K_2/K_1$) describes the strain-stiffening constitutive behavior of strands by relating the moduli of the first ($K_1$) and second regimes ($K_2$) of the force-length curve during loading to the failure force ($f_f$) and length ($L_f$). (c) Tuning the nonlinearity parameter ($K_2/K_1 \in [1, 10^4]$), stiffness crossover length ($L_x$), failure length ($L_f \in [1\text{ nm}, 1\text{ m}]$), and rupture force ($f_f \in [1\text{ nN}, 1\text{ N}]$) of single strands provides a breadth of candidates for network assembly and fracture testing. (d) Intrinsic fracture energy (normalized by the areal strand density $M$) scales linearly with $f_f$ and $L_f$ of single strands across all scales in a two-dimensional triangular lattice (loop size $n_{\text{loop}} = 3$), giving a prefactor $\alpha = 0.73$. (e) The scaling law holds for two-dimensional lattices with square ($n_{\text{loop}} = 4$) and hexagonal ($n_{\text{loop}} = 6$) lattices with prefactors $\alpha = 1.46$ and 2.54, respectively. Three-dimensional networks with (f) diamond cubic, (g) body-centered cubic, and (h) cubic unit cells follow the scaling law with $\alpha = 1.07$, 1.74, and 1.50, respectively.

networks, this additional energy can be dissipated by damping mechanisms such as viscous drag or friction. To quantitatively measure each energetic contribution, we first load a notched sample from the reference state until the bridging strand reaches $L_f$ [Fig. 2(a)(i) and 2(a)(ii)] and track the force-length response of that strand [Figs. 2(b)(i) and 2(b)(ii)]. Integration of this relation supplies the energetic contribution of a single strand $U_{\text{strand}}$. Upon abrupt rupture, we fix the boundary conditions and replace the bridging strand with a pair of opposing artificial forces between the two end points. We first prescribe the length between these end points to $L_f$ and calculate the reaction force required to preserve equilibrium. We then quasistatically increase the distance between the end points [Fig. 2(a)(ii)–(iv)] and record this force [Fig. 2(b)(ii)–(iv)] until its magnitude reaches zero, marking the new

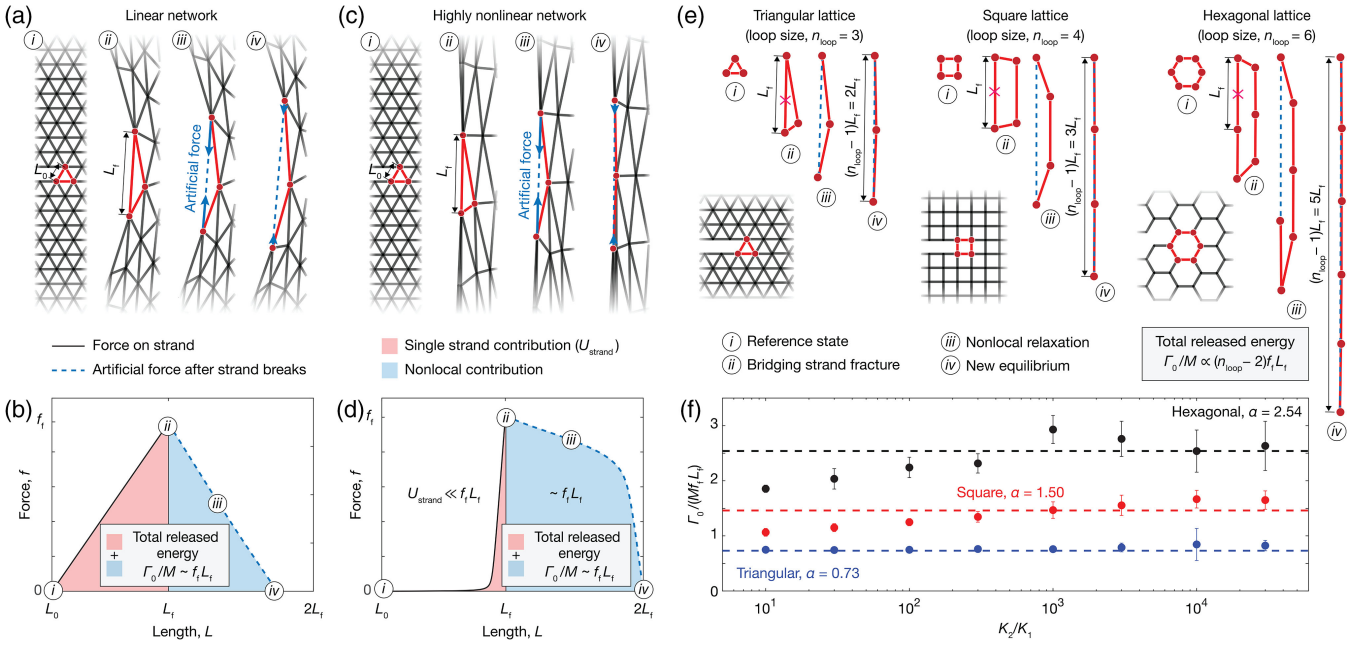


FIG. 2. Physical explanation of the scaling for intrinsic fracture energy of stretchable networks. (a) A case study simulates a notched triangular network of strands with linear mechanics ($K_2/K_1 \approx 1$) and loads from the undeformed state (i) until bridging strand fracture and (ii) then quasistatically reduces artificial forces on the ends of the broken strand (iii) until the network reaches equilibrium (iv). (b) The integration of the tracked strand loading force (red) and nonlocal energy release (blue) as a function of length between strand ends explains the critical energy release rate $G_c$ to break the bridging strand. This quantity aligns with the measured $\Gamma_0/M$ and scales with $f_f L_f$ in elastic networks. (c) A second case study repeats the procedure for a network of strands with high nonlinearity ($K_2/K_1 \approx 10^4$) but the same $f_f$ and $L_f$. (d) While the single-strand energy ($U_{\text{strand}}$, red) is much smaller than $f_f L_f$, the total integration of the single strand and nonlocal contributions counterbalance and scale with $f_f L_f$. (e) Simulation results depict extension from triangular ($n_{\text{loop}} = 3$) to square ($n_{\text{loop}} = 4$) and hexagonal ($n_{\text{loop}} = 6$) lattices for strands with high nonlinearity ($K_2/K_1 \approx 10^4$). The measured $\alpha$ parameter scales with the relaxation length or difference between $(n_{\text{loop}} - 1)L_f$ and $L_f$ [i.e., $\alpha \sim (n_{\text{loop}} - 2)$]. All results are numerically derived from simulations. (f) Measured $\Gamma_0/M$ normalized by $f_f L_f$, which gives $\alpha$, is plotted against $K_2/K_1$ across lattices.

unperturbed network equilibrium. Integration of this relaxation response yields the energy released by the network continuum. Together, the sum of both responses [Fig. 2(b)(i)–(iv)] gives the critical energy release rate $G_c$ supplied by the loading condition, which aligns with $\Gamma_0$ in elastic networks studied here. This conceptually parallels the crack closure integral from linear elastic fracture mechanics, which enables evaluation of energy release rates $G$ from stress intensity factors [41–43]. Therefore, this numerical result quantitatively describes the energetic contributions of the single strand (red region) and network continuum (blue region) to the measured intrinsic fracture energy (see Appendix B 3 for simulation details).

During postfracture relaxation, the network exerts reaction forces $\propto f_f$ across a distance $\propto L_f$ on the broken strand ends. For networks with linear strands [Fig. 2(a)], the bridging strand and nonlocal contributions are on the same order of magnitude [Fig. 2(b), red region], so $\Gamma_0/M \propto U_{\text{strand}}$ still provides a reasonable approximation. However, this does not hold when applied to networks with highly nonlinear strands [Fig. 2(c)]; the single-strand contribution constitutes only a small fraction of the total released energy [Fig. 2(d)]. Instead, the released energy from the network continuum dominates, which is consistent with findings from our recent work [25]. Also, in networks with increasingly nonlinear strands, more strands are highly stretched, which deconcentrates stress from the crack tip. Therefore, the total measured intrinsic fracture energy of the network always scales with $f_f L_f$.

Next, we investigate how different types of networks affect the fitting parameter $\alpha$ in the scaling law. The key topological parameter describing a lattice during fracture is its loop size: the number of strands within the shortest closed path; our analysis includes triangular (loop size, $n_{\text{loop}} = 3$), square ($n_{\text{loop}} = 4$), and hexagonal ($n_{\text{loop}} = 6$) lattices.

As shown in Fig. 2(e), the loop connected to the bridging strand in the notched sample opens when the strand breaks at $L_f$, stretching and aligning the strands within that loop. The broken strand ends in triangular, square, and hexagonal lattices migrate in this process from a distance of $L_f$ to about $2L_f$, $3L_f$, and $5L_f$, respectively. The relaxation length, defined as the difference between the fully extended and initial loop lengths [$(n_{\text{loop}} - 1)L_f$ and $L_f$, respectively], generally yields $(n_{\text{loop}} - 2)L_f$.

This result establishes a topological interpretation for the parameter $\alpha$ as $\alpha \propto (n_{\text{loop}} - 2)$, providing a more explicit form of the scaling law:

$$\Gamma_0/M \propto (n_{\text{loop}} - 2) f_f L_f. \tag{3}$$

To distinguish simulation results across topologies and strand nonlinearities, we normalize $\Gamma_0/M$ by the scaling law $f_f L_f$, which gives $\alpha$, and plot the results against $K_2/K_1$ [Fig. 2(f)]. Loop size directly affects $\alpha$, which is consistent with our model. While loop size becomes more complex in three-dimensional networks due to structural intricacies (i.e., strands with multiple adjoining loops, etc.), effective loop sizes can be found which match this result.

## V. EXPERIMENTAL VERIFICATION

We illustrate the versatility and consistency of this scaling through experimental validation across a spectrum of networks, ranging from architected materials composed of strands at the millimeter level to polymers composed of strands at the nanometer level. For macroscale architected materials, we fabricate two- and three-dimensional networks from folded and spring-shaped strands, respectively, with various strain-stiffening $K_2/K_1$ behaviors by controlling the transition between compliant unfolding ($K_1$) and stiffer material stretching ($K_2$) during loading. Two-dimensional triangular lattices of repeating strands are laser cut (model: Epilog Laser Fusion Maker 12) from polyester (0.001″ thick) and polyacetal (0.003″ and 0.005″ thick) films (McMaster-Carr) [Fig. 3(a)]. Three-dimensional diamond lattices of repeating strands are modeled in a commercial 3D modeling software (SolidWorks, Dassault Systems) and 3D printed (Inkbit Vista, Inkbit) using a thiol-ene polyurethane elastomer (TEPU30A, Inkbit) [44] [Fig. 3(b)]. Intrinsic fracture energy is calculated after loading an unnotched specimen in pure shear to obtain the force-stretch behavior and extending notched specimens in pure shear to the critical height $h_c$ where bridging strands reach $L_f$. For nanoscale polymer networks, we collect intrinsic fracture energy measurements from across the literature [45–47] for tetra-poly(ethylene glycol) (PEG) hydrogels, since they possess relatively homogeneous networks [48]. Degree of polymerization $N$ between cross-links tunes the failure length of polymer strands ($L_f \sim N$) [45], while mechanophores embedded in the backbone tune the rupture force of strands $f_f$ [47]. Representative force-length relations parametrized from experiments by the m-FJC model for polymer network strands are plotted in the left column in Fig. 3(c). The parameters and detailed calculations can be found in the Supplemental Material [36] (Sec. S2.2).

These experimental networks cover a vast spectrum of single-strand nonlinearity parameters ($K_2/K_1$ from 20 to $1.8 \times 10^4$), breaking forces ($f_f$ from 1.3 nN to 1.7 N), and

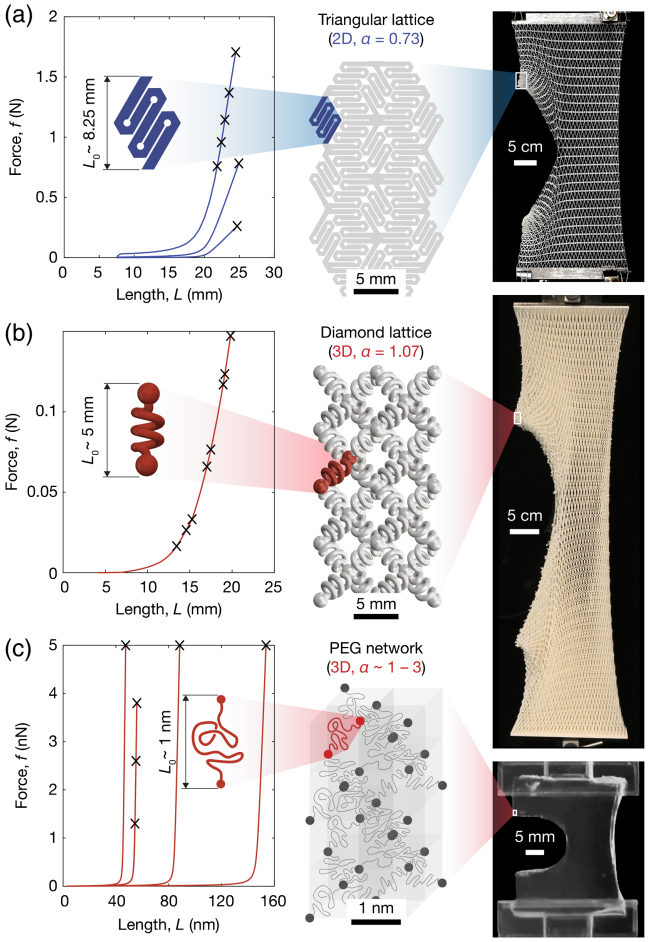


FIG. 3. Experimental networks for fracture tests. (a) Macroscale two-dimensional architected triangular networks, (b) macroscale three-dimensional architected diamond-lattice networks, and (c) nanoscale three-dimensional poly(ethylene glycol) end-linked polymer networks [45–47] are fabricated to measure intrinsic fracture energy $\Gamma_0$. The left column displays the force-length relations for single strands during mechanical loading from the undeformed strand length $L_0$ to the fracture length $L_f$ and fracture force $f_f$. Failure points of various strand designs are denoted by black markers. The crossover length $L_x$ and nonlinearity parameter $K_2/K_1$ can be calculated or fit to describe these behaviors via the m-FJC model. The center column displays the topologies and length scales of repeating units within bulk samples and the predicted scaling parameter $\alpha$ from simulations. The rightmost images display notched samples loaded to the critical height $h_c$ during the pure shear fracture test. Unnotched samples are loaded past $h_c$ to measure $\Gamma_0$ for validation of the scaling law.

breaking lengths ($L_f$ from 47.4 nm to 25.1 mm). Across this range, the proposed scaling law predicts the experimentally measured polymer [Fig. 4(a)] and architected [Fig. 4(b)] network intrinsic fracture energy. Overall, experimental agreement of nanoscale polymer networks and macroscopic architected materials to the scaling law synergistically promote its applicability in predicting diverse network fracture [Fig. 4(c)].

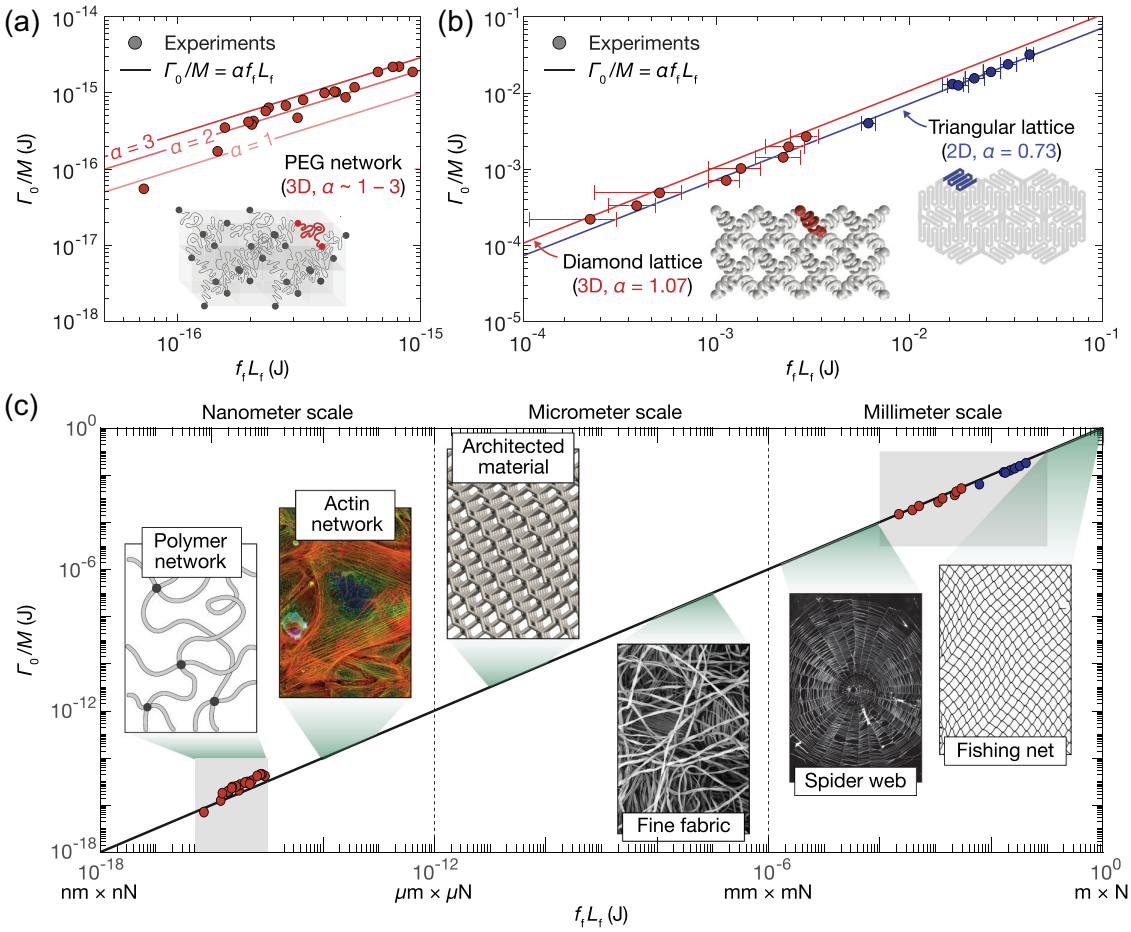


FIG. 4. Intrinsic fracture energy in experimental networks. Experiments validate the scaling law in predicting the measured intrinsic fracture energies of networks ranging from (a) nanoscale three-dimensional PEG polymer networks from the literature to (b) macroscale two- and three-dimensional architected networks with various single-strand behaviors. (c) Experimental results show the applicability of the scaling law to a vast range of materials across scales, including polymer networks, biological networks (image courtesy of Howard Vindin), architected materials, textiles (image courtesy of E. P. Vicenzi from Smithsonian's Museum Conservation Institute and National Institute of Standards and Technology), spider webs (image courtesy of Chen-Pan Liao), and nets (image courtesy of Nikodem Nijaki).

## VI. DISCUSSION

The scaling law presented here highlights that the intrinsic fracture energy of a breadth of network materials directly depends on loop size and fracture force. First, strand lengths (via $L_f$) and connectivity (via $\alpha$) describe the loop size in the network. Bridging strand rupture propagates a crack by unfolding the surrounding loop of strands. The extent to which the loop opens dictates the energy release from the continuum network. This finding suggests that networks designed with longer strands or larger topological loops can result in increased toughness per broken chain. Second, the dependence of the scaling law on strand fracture force underscores that the effect of strand constitutive behavior is minor. Given a constant fracture force for topologically equivalent networks, measurements indicate that changing the shape of the force-length loading profile to reach the strand rupture point does not significantly vary the intrinsic fracture energy. This result deviates from the long-standing notion that intrinsic fracture energy scales with $U_{\text{strand}}$. It also surprisingly unifies fracture in networks expressing different failure physics. Energy release is local to the crack tip in linear networks yet nonlocal in nonlinear networks; nonetheless, both types obey the scaling law.

The topological parameter $\alpha$ approximated by loop size aligns well with experimental outcomes. The PEG polymer network results match with $\alpha$ between 1 and 3 and scale appropriately [Fig. 4(a)]. The $\alpha$ value of 0.73 from triangular lattice simulations shows strong agreement with the experiments for two-dimensional architected triangular networks; similarly, the value of 1.07 from diamond lattice simulations matches well with experiments for three-dimensional architected diamond networks [Fig. 4(b)]. While networks containing heterogeneities require further exploration, these results highlight the relevance of the scaling law to latticelike systems. The relatively homogeneous tetra-PEG gel case presented here suggests that this scaling law could potentially apply to the molecular level.

The findings shared in this work parallel a separate phenomenon studied in linear elastic fracture mechanics called lattice trapping [49]. Lattice models implementing atomistic force laws to approximate fracture of atomically bonded materials expose a mismatch in the measured critical energy release rate for crack propagation and the surface energy dissipated by breaking bonds [50]. This mismatch occurs because the lattice structure exhibits an energy barrier which traps the network in a local energy minimum even though the fractured state is the global energy minimum. The nonlocal contribution to intrinsic fracture energy parallels this lattice trapping effect. For real crystalline materials, this energy barrier typically remains small enough such that the combination of thermal energy, dislocations, grain structure, etc., causes the crack to overcome the barrier to fracture within relevant timescales [51,52]. For networks described here, this energy barrier can become extremely steep. We contend that the crack would likely not overcome this barrier on relevant timescales due to thermal fluctuations or structural defects. The true impact of energy fluctuations on lattice trapping across all networks and length scales remains an open question. We propose that the full local and nonlocal effects must be considered together to capture the intrinsic fracture energy measured in networks studied here.

Interestingly, the model developed here can reasonably account for the fracture of unentangled, semidilute polymer gels. Unlike architected materials, polymer networks are more complex and inherently involve polydispersity. The chain length between cross-links, the size of topological loops, and the strand scission force all follow distributions. Despite this complexity, the experimental data can be semiquantitatively captured with the prefactor $\alpha$, which is proportional to the size of topological loops. How polydispersity influences the developed model, however, still requires further investigation.

Networks manifest in nature due to exceptional resistance to failure under harsh loading conditions. Designing materials that mechanistically resist fracture requires an understanding of the hierarchical connection between strand mechanics, network connectivity, and macroscopic properties. Here, we reveal a simple scaling that unifies the fracture of networks across many length scales, strand mechanical nonlinearities, and lattice topologies. Advancing a crack through a network requires local energy dissipation through breaking the bridging strand and nonlocal energy release through opening the adjoining loop to rebalance. When strands exhibit nearly linear force-length relationships, energy dissipation is local to the crack tip. When strands exhibit highly nonlinear relationships, the nonlocal energy release can far exceed the elastic energy contained within the bridging strand. In each case, the physical process counterintuitively gives a measured intrinsic fracture energy that scales with geometry through $n_{\text{loop}}$ and single-strand mechanics through $f_f L_f$ instead of $U_{\text{strand}}$. These findings provide a foundational mechanism for interpreting and designing networks as tough materials. For instance, nanoscale polymer strands garner toughness in natural, biological, and synthetic networks by synergistically achieving high deformations and rupture forces. Similarly, animals such as bees and spiders leverage connectivity to resist honeycomb and web fracture. This scaling law not only elucidates the beauty of existing network structures, but informs future design of lattices in metamaterials, textiles, and beyond.

## ACKNOWLEDGMENTS

The authors acknowledge the MIT SuperCloud and Lincoln Laboratory Supercomputing Center for providing HPC resources that have contributed to the research results reported within this paper. This work was supported in part by the National Institutes of Health (Grants No. 1R01HL153857-01 and No. 1R01HL167947-01), Department of Defense Congressionally Directed Medical Research Programs (Grant No. PR200524P1), and the National Science Foundation (Grant No. EFMA-1935291). C. M. H. acknowledges support from the NSF Graduate Research Fellowship and the MathWorks Fellowship.

## APPENDIX A: COMPUTATIONAL METHODS

### 1. Mathematical model for numerical simulation

We model networks as systems of connected nonlinear elastic springs with constitutive force $f$ and length $L$ relations characterized by the modified freely jointed chain model in Eq. (2). This formula yields the constitutive law we apply to each nonlinear spring in the simulation. To capture strand rupture, a breaking force $f_f$ and length $L_f$ are prescribed to the spring. We vary the range of $f_f$ from 1 nN to 1 N, $L_f$ from 1 nm to 1 m, and $K_2/K_1$ from 1 to $3.0 \times 10^4$ to broadly describe networks across scales. High nonlinearity parameters capture the extreme strain-stiffening behavior measured using single molecule force spectroscopy for common polymers such as poly(acrylic acid) [53], poly(vinyl alcohol) [54], polyisoprene [55], poly(acryl amide) and poly(N-isopropyl acrylamide) [56], poly(dimethylacrylamide) and poly(diethylacrylamide) [57], and poly(ethylene glycol), whose nonlinearity parameter reaches upward of $1.8 \times 10^4$ [58]. The breaking length $L_f$ is notably selected in simulations to be at least 5 times the initial length (i.e., $L_f > 5L_0$) to limit geometric artifacts.

We describe the lattice deformation of general three-dimensional networks consisting of $n$ nodes and $e$ edges through their coordinates $(x_i, y_i, z_i)$, where $i = 1, \ldots, n$. Two matrices store the node coordinates and their respective connectivities in MATLAB. The total system energy at

each loading step is expressed as the sum of the elastic energy stored in each edge or spring as

$$U_{\text{total}} = \sum_{i,j} \int_1^{\lambda_{ij}} f(\lambda')d\lambda', \tag{A1}$$

where $\lambda_{ij}$ is the stretch of the edge connecting node $i$ with $j$:

$$\lambda_{ij} = r_0^{-1}\sqrt{(x_i - x_j)^2 + (y_i - y_j)^2 + (z_i - z_j)^2}. \tag{A2}$$

Minimizing $U_{\text{total}}$ numerically provides the coordinates of each node $(x_i, y_i, z_i)$ as solved by equating

$$\frac{\partial U_{\text{total}}}{\partial x_i} = 0, \qquad \frac{\partial U_{\text{total}}}{\partial y_i} = 0, \qquad \frac{\partial U_{\text{total}}}{\partial z_i} = 0, \tag{A3}$$

using Newton's method in MATLAB. Additionally, a broken edge between nodes $i$ and $j$ is detected when $\lambda_{ij} > \lambda_f$ and removed by deleting the corresponding entries of the connectivity matrices.

Clamped boundary conditions are prescribed in the simulation to the top and bottom surface to quasistatically stretch the sample from the initial height $h_0$ to a final height $h$ in the $y$ direction. The displacement boundary condition is applied in the simulation on the top and bottom nodes as

$$\begin{aligned} y_i &= h, \quad \text{for } i \in \text{top nodes}, \\ y_i &= y_i^0, \quad \text{for } i \in \text{bottom nodes}, \end{aligned} \tag{A4}$$

where $y_i^0$ denotes the initial $y$ position of the $i$th nodes.

The sample width $w_0$ in the $x$ direction is set to twice the height $h_0$ in all simulations as $w_0 = 2h_0$. We fix the $x$ displacement on the left and right boundaries to enforce a pure shear loading condition and limit edge effects via

$$\begin{aligned} x_i &= x_i^0, \quad \text{for } i \in \text{left nodes}, \\ x_i &= x_i^0, \quad \text{for } i \in \text{right nodes}, \end{aligned} \tag{A5}$$

where $x_i^0$ denotes the initial $x$ position of the $i$th nodes. Equations (A3)–(A5) form a boundary value problem that can be solved numerically.

### 2. Quasistatic solver

The node coordinates $(x_i, y_i, z_i)$ fully describe the state of the system, so all variables can be rewritten as vectors:

$$\mathbf{X} = [x_1, y_1, z_1, x_2, y_2, z_2, \ldots, x_n, y_n, z_n]^T. \tag{A6}$$

The $3n$ by 1 vector $\mathbf{X}$ contains all necessary information to describe the lattice deformation. The nonlinear system of equations described in Eqs. (A3)–(A5) is solved to obtain $\mathbf{X}$ and can be written generally as

$$\mathbf{F}(\mathbf{X}) = \mathbf{0}. \tag{A7}$$

Note that the equation above presents the same governing equations depicted in Eq. (A3).

The solver implements Newton's method to solve the governing equation [Eq. (A7)]. The generalized Newton's method is to find a root of a functional $\mathbf{F}$ defined in a Banach space. In this case, the formulation is

$$\mathbf{X}_{l+1} = \mathbf{X}_l - [\mathbf{J}(\mathbf{X}_l)]^{-1}\mathbf{F}(\mathbf{X}_l), \tag{A8}$$

where $\mathbf{J}(\mathbf{X}_l)$ is the Jacobian matrix of the function $\mathbf{F}$ at $\mathbf{X}_l$ and $l$ is the iteration number. Instead of computing the inverse of this matrix, one can save time by solving the following system of linear equations:

$$\mathbf{J}(\mathbf{X}_l)(\mathbf{X}_{l+1} - \mathbf{X}_l) = -\mathbf{F}(\mathbf{X}_l). \tag{A9}$$

Starting with an initial guess $\mathbf{X}_0$, the next approximate solution $\mathbf{X}_l$ is obtained iteratively. The method ends when $\|\mathbf{X}_{l+1} - \mathbf{X}_l\| < \delta$, where $\delta$ is a defined accuracy requirement.

The quasistatic simulation divides the loading process into $P$ steps to gradually stretch the network. It obtains the system state $\mathbf{X}^{(p)}$ by solving Eq. (A7), where $p = 1, \ldots, P$, at each step. To accelerate convergence of Newton's method, the solution of the current step provides the initial guess for the upcoming step. Upon breaking a bridging strand at step $p$ during loading to measure $\Gamma_0$, the solver maintains the boundary conditions (i.e., $h = h_c$), searches for a new equilibrium state, and checks for strand fracture before continuing to $p + 1$.

### 3. Postrupture artificial force decay simulation

We adapt the simulation protocol to explore the physical explanation for the scaling law by tracking and relaxing the nodes connecting the first bridging strand following rupture. A notched network is first loaded to the critical height $h_c$ where the first bridging strand breaks. The bulk boundary conditions are fixed for the remainder of the simulation. Instead of breaking the bridging strand and equilibrating the system, the strand is replaced by an approximately infinitely stiff spring ($K_{\text{spring}} \gg K_2 \geq K_1$). At the initial step, the simulation fixes the length of the stiff spring to match the length of the broken strand ($L_{\text{spring}} = L_f$), obtains the next system state $\mathbf{X}^{(P+1)}$ by solving Eq. (A7), and stores the pair of opposing artificial forces required to preserve equilibrium on each node. For the remaining steps, the algorithm incrementally lengthens the spring, equilibrates the system state, and stores the new spring force readout. The iterative procedure concludes once the measured spring force reaches a small tolerance of zero or the spring reaches a predetermined terminal length.

### 4. Coarse-graining simulation procedure

We simulate networks on the order of thousands of layers to ensure convergence of samples with high nonlinearity

parameters (see Supplemental Material [36] for details on convergence). Networks are coarse-grained far from the crack tip for computational efficiency (see Supplemental Material [36] for a case study on the computational limits). The coarse-grained method reconstructs large networks with drastically fewer degrees of freedom (DOFs). Near fracture of the bridging strand, the network is most inhomogeneous near the crack tip but becomes more homogeneous with increasing distance. Since strands far from the crack tip do not substantially vary in their local neighborhoods, a coarse lattice can equivalently describe their continuum-level mechanical response. For instance, a two-dimensional triangular network with $h_0 = 100$ layers and $w_0 = 200$ layers can be reconstructed with incremental levels of coarse lattices moving radially outward from the crack tip (see the Supplemental Material [36] figure on coarse-graining). The relative stiffness of coarse-grained strands is prescribed proportionally to length (represented by line thicknesses in the Supplemental Material [36] figure on coarse-graining) to ensure the coarse-grained neighborhoods maintain the same bulk mechanical performance as the full network. In notched samples, levels incrementally coarsen with increasing distance in the $x$ and $y$ directions from the undeformed crack tip. A full two-dimensional network possessing 23 057 nodes can, therefore, be coarse-grained with this scheme to contain only 1047 nodes (see Supplemental Material [36] figure on coarse-graining). Direct comparisons indicate that the coarse-grained model accurately predicts the critical stretch at which the first strand breaks (see Supplemental Material [36] for a detailed comparison). While the coarse-grained model cannot accurately capture the full fracture process, it yields an accurate measure of $h_c$ in the pure shear fracture test.

The coarse-grained triangular networks used for all simulations contain a size of $h_0 = 4000$ layers by $w_0 = 8000$ layers, with a total of 44 847 nodes and 89 694 DOFs (see the Supplemental Material [36] figure on coarse-grained sample size). Note that an equivalent full network requires about 40 million nodes; the coarse-graining scheme decreases the required number by 99.9%. Each iteration of Newton's method—which includes assembling the Jacobian matrix and solving Eq. (A8)—typically costs a few seconds. The full fracture simulation of a two-dimensional $h_0 = 4000$ layer network typically takes under 20 min to complete on a standard desktop with Intel Core i9- 12900K.

## APPENDIX B: EXPERIMENTAL METHODS

### 1. Fabrication of two-dimensional architected networks

Two-dimensional networks are fabricated by laser cutting polyester (12" × 12" × 0.001") and polyacetal (12" × 12" × 0.003", 0.005") sheets (McMaster-Carr part numbers 7594T11 and 5742T11) with a laser cutter (Fusion Maker 12, Epilog Laser). The triangular network strand pattern is designed (CorelDRAW, Corel Corporation) with 28 vertical layers of repeating units with 60 strands per layer. Each strand has a "zigzag" structure that unfolds to provide an initial compliant bending regime then deforms the material to provide a final stiff stretching regime [59]. This large discrepancy between stiffness enables high values and tunability of the nonlinearity parameter $K_2/K_1$ from the m-FJC model. The distance between the laser head and the acetal film is calibrated before cutting to ensure sharp focus. Cutting parameters are selected to be 10% for laser power, 10% for frequency, and 100% for speed. Four identical samples in total are cut to perform each measurement of energy release rate. For each sample, four 1/16" acrylic sheets are cut and glued on either side of an uncut portion at the top and bottom of the sample to act as a rigid boundary, which is clamped onto the mechanical testing machine.

### 2. Fabrication of three-dimensional architected networks

For three-dimensional networks, single spring-shaped strands are designed and parametrized using commercial 3D modeling software (Solidworks, Dassault Systems). Strands are assembled spatially into a diamond cubic unit cell and joined at strand ends via spherical nodes. Unit cells comprised of 16 strands are patterned into a $16 \times 16 \times 8$ array. The resulting lattice contains 2048 unit cells and 32 768 single strands. Rectangular plates are joined to the top and bottom faces of the network. The assembled components are joined and resized such that single strands are 5 mm in length, giving a bulk height of 186 mm for the 16 unit cells. The resulting network is saved as a stereolithography file, exported, and 3D printed on a vision controlled jetting system (Inkbit Vista, Inkbit) using a thiolene polyurethane elastomer (TEPU30A, Inkbit). For each sample, four acrylic sheets are cut and glued to the top and bottom plates to form a rigid boundary with a vertical protrusion to be clamped onto the testing machine.

### 3. Experimental measurement of two-dimensional architected networks

Pure shear fracture tests are performed on two-dimensional networks using a ZwickiLine materials testing machine (2.5 kN load cell, Zwick/Roell). To measure fracture energy $\Gamma_0$, a uniaxial extension test is first performed on a pristine sample at a constant loading rate of 100 mm/ min. Using the experimentally obtained uniaxial response, we inversely identify the effective force-length curve for each strand such that the simulation results match experiments. We first simulate the uniaxial loading response for an identical sample geometry and topology, with strands exhibiting a J-shaped force-length response estimated to mimic the expected behavior for the ribbon-shaped strands. We then tune the parameters of the m-FJC model and repeat the loading scheme until the simulation

results for an unnotched network match experiments. To validate this approach, five individual 0.005" polyacetal strands are laser cut and tested uniaxially. The average force-length curve measured experimentally matches the profile obtained by the inverse method. The inverse method is then used for 0.003" polyacetal and 0.001" polyester two-dimensional networks, along with three-dimensional samples (see Appendix B 4 and Figs. S10–S12 [36]). For the remaining three samples, we introduce an identical edge crack with length $\sim w_0/2$ perpendicular to the loading direction. Uniaxial tensile tests are performed on the three notched samples at a loading rate of 100 mm/ min. Since the rupture of strands is uncontrolled when a notched sample is loaded to the fracture event, we preset the critical stretched height $h_c$ and consider the bridging strands to "rupture" when the whole network reaches that applied height. The energy release rate of the pristine sample at $h = h_c$ is measured and recorded. The intrinsic fracture energy $\Gamma_0$ of the network is computed by integrating the stress-height behavior of the unnotched sample to $h = h_c$ as $\Gamma_0 = \int_{h_0}^{h_c} sdh$ [Fig. S12(b) [36] ]. The rupture length $L_f$ of the bridging strand is measured using calipers when the notched sample reaches $h_c$ [Fig. S12(a) [36] ], and the rupture force $f_f$ is interpolated from the single-strand force-length curve [Fig. S12(c) [36] ].

### 4. Experimental measurement of three-dimensional architected networks

Three-dimensional pure shear tests are performed using a single-axis Instron universal testing machine (500N load cell, Instron 5566) at a constant loading rate of 1 mm/s. Prior to mechanical loading, rigid acrylic mounts are glued to the rectangular plates printed on the top and bottom faces of the sample. Mounts are then fixed via mechanical grippers within the testing apparatus. The fracture energy $\Gamma_0$ is calculated by the same procedures outlined for the two-dimensional networks (see Appendix B 3), unless otherwise noted. Note that crack of width $w_0/2$ is cut through all layers in the thickness direction. The rupture lengths $L_f$ of the bridging strand are measured based on snapshots of experimental recordings at different critical sample heights $h_c = h$ (see Fig. S11 [36]). At each loading state, we measure five bridging strands in the thickness direction and take their average as the current $L_f$. Note that, due to gravity, the strands fall on each other at the original height of 186 mm. The network is not fully opened until it has been stretched to 350 mm. To eliminate the effect of gravity, we set the measured force to 0 N until the network is stretched to 350 mm.


[1] Yuval Mulla, Mario J. Avellaneda, Antoine Roland, Lucia Baldauf, Wonyeong Jung, Taeyoon Kim, Sander J. Tans, and Gijsje H. Koenderink, *Weak catch bonds make strong networks*, Nat. Mater. **21**, 1019 (2022).

[2] Federica Burla, Simone Dussi, Cristina Martinez-Torres, Justin Tauber, Jasper van der Gucht, and Gijsje H. Koenderink, *Connectivity and plasticity determine collagen network fracture*, Proc. Natl. Acad. Sci. U.S.A. **117**, 8326 (2020).

[3] Elena Kassianidou, Christoph A. Brand, Ulrich S. Schwarz, and Sanjay Kumar, *Geometry and network connectivity govern the mechanics of stress fibers*, Proc. Natl. Acad. Sci. U.S.A. **114**, 2622 (2017).

[4] Daisuke Mizuno, Catherine Tardin, Christoph F. Schmidt, and Frederik C. MacKintosh, *Nonequilibrium mechanics of active cytoskeletal networks*, Science **315**, 370 (2007).

[5] Ovijit Chaudhuri, Sapun H. Parekh, and Daniel A. Fletcher, *Reversible stress softening of actin networks*, Nature (London) **445**, 295 (2007).

[6] Timothée Vignaud, Calina Copos, Christophe Leterrier, Mauricio Toro-Nahuelpan, Qingzong Tseng, Julia Mahamid, Laurent Blanchoin, Alex Mogilner, Manuel Théry, and Laetitia Kurzawa, *Stress fibres are embedded in a contractile cortical network*, Nat. Mater. **20**, 410 (2021).

[7] Chase M. Hartquist, Shaoting Lin, James H. Zhang, Shu Wang, Michael Rubinstein, and Xuanhe Zhao, *An elastomer with ultrahigh strain-induced crystallization*, Sci. Adv. **9**, eadj0411 (2023).

[8] Qi Li, John Kulikowski, David Doan, Ottman A. Tertuliano, Charles J. Zeman IV, Melody M. Wang, George C. Schatz, and X. Wendy Gu, *Mechanical nanolattices printed using nanocluster-based photoresists*, Science **378**, 768 (2022).

[9] Tobias Frenzel, Muamer Kadic, and Martin Wegener, *Three-dimensional mechanical metamaterials with a twist*, Science **358**, 1072 (2017).

[10] Terry C. Shyu, Pablo F. Damasceno, Paul M. Dodd, Aaron Lamoureux, Lizhi Xu, Matthew Shlian, Max Shtein, Sharon C. Glotzer, and Nicholas A. Kotov, *A kirigami approach to engineering elasticity in nanocomposites through patterned defects*, Nat. Mater. **14**, 785 (2015).

[11] Yun Ling, Wenbo Pang, Jianxing Liu, Margaret Page, Yadong Xu, Ganggang Zhao, David Stalla, Jingwei Xie, Yihui Zhang, and Zheng Yan, *Bioinspired elastomer composites with programmed mechanical and electrical anisotropies*, Nat. Commun. **13**, 524 (2022).

[12] Jianxing Liu, Dongjia Yan, Wenbo Pang, and Yihui Zhang, *Design, fabrication and applications of soft network materials*, Mater. Today **49**, 324 (2021).

[13] Carter S. Haines, Márcio D. Lima, Na Li, Geoffrey M. Spinks, Javad Foroughi, John D. W. Madden, Shi Hyeong Kim, Shaoli Fang, Mônica Jung de Andrade, Fatma Göktepe *et al.*, *Artificial muscles from fishing line and sewing thread*, Science **343**, 868 (2014).

[14] George C. Engelmayr, Jr., Mingyu Cheng, Christopher J. Bettinger, Jeffrey T. Borenstein, Robert Langer, and Lisa E. Freed, *Accordion-like honeycombs for tissue engineering of cardiac anisotropy*, Nat. Mater. **7**, 1003 (2008).

[15] J. E. Bolander, Jr. and Shigehiko Saito, *Fracture analyses using spring networks with random geometry*, Eng. Fract. Mech. **61**, 569 (1998).

[16] Gianluca Cusatis, Daniele Pelessone, and Andrea Mencarelli, *Lattice discrete particle model (ldpm) for*

*failure behavior of concrete. I: Theory*, Cem. Concr. Compos. **33**, 881 (2011).
[17] G. Lilliu and Jan G. M. van Mier, *3d lattice type fracture model for concrete*, Eng. Fract. Mech. **70**, 927 (2003).
[18] Yifan Wang, Liuchi Li, Douglas Hofmann, José E. Andrade, and Chiara Daraio, *Structured fabrics with tunable mechanical properties*, Nature (London) **596**, 238 (2021).
[19] Costantino Creton and Matteo Ciccotti, *Fracture and adhesion of soft materials: A review*, Rep. Prog. Phys. **79**, 046601 (2016).
[20] Xuanhe Zhao, Xiaoyu Chen, Hyunwoo Yuk, Shaoting Lin, Xinyue Liu, and German Parada, *Soft materials by design: Unconventional polymer networks give extreme properties*, Chem. Rev. **121**, 4309 (2021).
[21] Angkur Jyoti Dipanka Shaikeea, Huachen Cui, Mark O'Masta, Xiaoyu Rayne Zheng, and Vikram Sudhir Deshpande, *The toughness of mechanical metamaterials*, Nat. Mater. **21**, 297 (2022).
[22] Naomi E. R. Romijn and Norman A. Fleck, *The fracture toughness of planar lattices: Imperfection sensitivity*, J. Mech. Phys. Solids **55**, 2538 (2007).
[23] Alan Arnold Griffith, *VI. The phenomena of rupture and flow in solids*, Phil. Trans. R. Soc. A **221**, 163 (1921).
[24] G. J. Lake and A. G. Thomas, *The strength of highly elastic materials*, Proc. R. Soc. A **300**, 108 (1967).
[25] Bolei Deng, Shu Wang, Chase Hartquist, and Xuanhe Zhao, *Nonlocal intrinsic fracture energy of polymerlike networks*, Phys. Rev. Lett. **131**, 228102 (2023).
[26] Steven B. Smith, Yujia Cui, and Carlos Bustamante, *Overstretching b-DNA: The elastic response of individual double-stranded and single-stranded DNA molecules*, Science **271**, 795 (1996).
[27] Yunwei Mao, Brandon Talamini, and Lallit Anand, *Rupture of polymers by chain scission*, Extreme Mech. Lett. **13**, 17 (2017).
[28] Brandon Talamini, Yunwei Mao, and Lallit Anand, *Progressive damage and rupture in polymers*, J. Mech. Phys. Solids **111**, 434 (2018).
[29] Alexander Hrennikoff, *Solution of problems of elasticity by the framework method*, J. Appl. Mech. **8**, A169 (1941).
[30] E. Schlangen and J. G. M. Van Mier, *Simple lattice model for numerical simulation of fracture of concrete materials and structures*, Mater. Struct. **25**, 534 (1992).
[31] Jincheng Lei, Ziqian Li, Shuai Xu, and Zishun Liu, *A mesoscopic network mechanics method to reproduce the large deformation and fracture process of cross-linked elastomers*, J. Mech. Phys. Solids **156**, 104599 (2021).
[32] Jincheng Lei and Zishun Liu, *A network mechanics method to study the mechanism of the large-deformation fracture of elastomers*, J. Appl. Phys. **132**, 135101 (2022).
[33] Ahmed Ghareeb and Ahmed Elbanna, *An adaptive quasi-continuum approach for modeling fracture in networked materials: Application to modeling of polymer networks*, J. Mech. Phys. Solids **137**, 103819 (2020).
[34] Tetsuo Yamaguchi, Yudai Onoue, and Yoshinori Sawae, *Topology and toughening of sparse elastic networks*, Phys. Rev. Lett. **124**, 068002 (2020).
[35] R. C. Picu and S. Jin, *Toughness of network materials: Structural parameters controlling damage accumulation*, J. Mech. Phys. Solids **172**, 105176 (2023).
[36] See Supplemental Material at http://link.aps.org/supplemental/10.1103/PhysRevX.15.011002 for relevant details for simulation and experimental procedures. It includes information on convergence, coarse-graining, artificial force measurement, orientation, dimensionality (2D and 3D), and single strand stretchability in simulations and specifics regarding testing of architected networks and analysis of polymer gel measurements in experiments.
[37] Tianhao Yang, Kenneth M. Liechti, and Rui Huang, *A multiscale cohesive zone model for rate-dependent fracture of interfaces*, J. Mech. Phys. Solids **145**, 104142 (2020).
[38] Shu Wang, Sergey Panyukov, Michael Rubinstein, and Stephen L. Craig, *Quantitative adjustment to the molecular energy parameter in the Lake-Thomas theory of polymer fracture energy*, Macromolecules **52**, 2772 (2019).
[39] Brandon H. Bowser, Shu Wang, Tatiana B. Kouznetsova, Haley K. Beech, Bradley D. Olsen, Michael Rubinstein, and Stephen L. Craig, *Single-event spectroscopy and unravelling kinetics of covalent domains based on cyclobutane mechanophores*, J. Am. Chem. Soc. **143**, 5269 (2021).
[40] Matthias Rief, Mathias Gautel, Filipp Oesterhelt, Julio M. Fernandez, and Hermann E. Gaub, *Reversible unfolding of individual titin immunoglobulin domains by AFM*, Science **276**, 1109 (1997).
[41] G. R. Irwin, *Handbuch der Physik* (Springer, Berlin, 1958), Vol. 6.
[42] Edmund F. Rybicki and Melvin F. Kanninen, *A finite element calculation of stress intensity factors by a modified crack closure integral*, Eng. Fract. Mech. **9**, 931 (1977).
[43] Ronald Krueger, *Virtual crack closure technique: History, approach, and applications*, Appl. Mech. Rev. **57**, 109 (2004).
[44] Thomas J. K. Buchner, Simon Rogler, Stefan Weirich, Yannick Armati, Barnabas Gavin Cangan, Javier Ramos, Scott T. Twiddy, Davide M. Marini, Aaron Weber, Desai Chen *et al.*, *Vision-controlled jetting for composite systems and robots*, Nature (London) **623**, 522 (2023).
[45] Yuki Akagi, Jian Ping Gong, Ung-il Chung, and Takamasa Sakai, *Transition between phantom and affine network model observed in polymer gels with controlled network structure*, Macromolecules **46**, 1035 (2013).
[46] Shaoting Lin, Jiahua Ni, Dongchang Zheng, and Xuanhe Zhao, *Fracture and fatigue of ideal polymer networks*, Extreme Mech. Lett. **48**, 101399 (2021).
[47] Shu Wang, Haley K. Beech, Brandon H. Bowser, Tatiana B. Kouznetsova, Bradley D. Olsen, Michael Rubinstein, and Stephen L. Craig, *Mechanism dictates mechanics: A molecular substituent effect in the macroscopic fracture of a covalent polymer network*, J. Am. Chem. Soc. **143**, 3714 (2021).
[48] Takamasa Sakai, Takuro Matsunaga, Yuji Yamamoto, Chika Ito, Ryo Yoshida, Shigeki Suzuki, Nobuo Sasaki, Mitsuhiro Shibayama, and Ung-il Chung, *Design and fabrication of a high-strength hydrogel with ideally homogeneous network structure from tetrahedron-like macromonomers*, Macromolecules **41**, 5379 (2008).

[49] Robb Thomson, C. Hsieh, and V. Rana, *Lattice trapping of fracture cracks*, J. Appl. Phys. **42**, 3154 (1971).
[50] N. Bernstein and D. W. Hess, *Lattice trapping barriers to brittle fracture*, Phys. Rev. Lett. **91**, 025501 (2003).
[51] William A. Curtin, *On lattice trapping of cracks*, J. Mater. Res. **5**, 1549 (1990).
[52] J. E. Sinclair, *The influence of the interatomic force law and of kinks on the propagation of brittle cracks*, Philos. Mag. **31**, 647 (1975).
[53] Hongbin Li, Bingbing Liu, Xi Zhang, Chunxiao Gao, Jiacong Shen, and Guangtian Zou, *Single-molecule force spectroscopy on poly (acrylic acid) by AFM*, Langmuir **15**, 2120 (1999).
[54] Hongbin Li, Wenke Zhang, Xi Zhang, Jiacong Shen, Bingbing Liu, Chunxiao Gao, and Guangtian Zou, *Single molecule force spectroscopy on poly (vinyl alcohol) by atomic force microscopy*, Macromol. Rapid Commun. **19**, 609 (1998).
[55] W. K. Zhang, *Nano-mechanical detection of single molecules*, Ph.D. thesis, Jilin University, 2002.
[56] Wenke Zhang, Shan Zou, Chi Wang, and Xi Zhang, *Single polymer chain elongation of poly (n-isopropylacrylamide) and poly (acrylamide) by atomic force microscopy*, J. Phys. Chem. B **104**, 10258 (2000).
[57] Chi Wang, Weiqing Shi, Wenke Zhang, Xi Zhang, Yukiteru Katsumoto, and Yukihiro Ozaki, *Force spectroscopy study on poly (acrylamide) derivatives: Effects of substitutes and buffers on single-chain elasticity*, Nano Lett. **2**, 1169 (2002).
[58] F. Oesterhelt, M. Rief, and H. E. Gaub, *Single molecule force spectroscopy by AFM indicates helical structure of poly (ethylene-glycol) in water*, New J. Phys. **1**, 6 (1999).
[59] Kyung-In Jang, Ha Uk Chung, Sheng Xu, Chi Hwan Lee, Haiwen Luan, Jaewoong Jeong, Huanyu Cheng, Gwang-Tae Kim, Sang Youn Han, Jung Woo Lee *et al.*, *Soft network composite materials with deterministic and bio-inspired designs*, Nat. Commun. **6**, 6566 (2015).